Evaluation of Anthropogenic Influences on Atmospheric Oxygenated Organic Molecules in Both Gas and Particle Phases over the Southeastern Tibetan Plateau

Ying Yu[1,2,#], Song Guo[*,1,2], Rui Tan[1], Xinshi Ni[1], Zichao Wan[1], Chunxiang Ye[1], and Min Hu[1]

[1] *State Key Laboratory of Regional Environment and Sustainability, International Joint Laboratory for Regional Pollution Control, Ministry of Education (IJRC), College of Environmental Sciences and Engineering, Peking University, Beijing, 100871, China*

[2] *Collaborative Innovation Center of Atmospheric Environment and Equipment Technology, Nanjing University of Information Science & Technology, Nanjing 210044, China*

 # now at Institute of Climate and Energy Systems, Troposphere (ICE-3), Forschungszentrum Jülich, 52428, Germany

Corresponding author:

[*]Song Guo - State Key Laboratory of Regional Environment and Sustainability, International Joint Laboratory for Regional Pollution Control, Ministry of Education (IJRC), College of Environmental Sciences and Engineering, Peking University, Beijing, 100871, China; Email: songguo@pku.edu.cn

Abstract:

The Tibetan Plateau (TP), as the region with the highest altitude in the world, plays an important role in regulating climate change, and is highly sensitive to anthropogenic pollutants. To assess the impact of anthropogenic emissions on atmospheric oxygenated organic molecules (OOMs) and regional air quality in the southeastern TP, we conducted intensive field observations using iodide Chemical Ionization Mass Spectrometry combined with a Filter Inlet for Gases and AEROsols (FIGAERO-CIMS) during the @Tibet field campaigns. We detected 653 distinct OOMs in both gas and particle phases, with most falling within the intermediate volatility range. Supervised machine learning was used to classify OOMs based on precursor origin, including biogenic (isoprene and monoterpenes) and anthropogenic (aromatics and aliphatics) sources. Notably, OOMs derived from anthropogenic emissions dominated the measured compounds, representing 32.5% in the gas phase and 45.6% in the particle phase, substantially exceeding the contributions from biogenic sources (27.5% and 21.8% in the gas and particle phases, respectively). These results reveal the significant influence of anthropogenic emissions on atmospheric species even in remote areas, highlighting the urgent need to consider these impacts in future air quality assessments and pollution mitigation strategies in the TP region.

Keywords:

Tibetan Plateau (TP); Chemical Ionization Mass Spectrometry with a Filter Inlet for

Gases and AEROsols (FIGAERO-CIMS); Anthropogenic Emissions; Oxygenated Organic Molecules (OOMs); Machine Learning Approach

Synopsis:

Our work enhances our understanding of atmospheric pollutants and highlights the importance of anthropogenic sources to OOMs formation in the southeastern TP.

1. INTRODUCTION

Organic aerosols (OA) constitute a significant fraction of fine particulate matter globally,[1] adversely affecting air quality,[2] climate,[3] and human health.[4] The complexity of OA, especially secondary organic aerosols (SOA), complicates our understanding of their chemical compositions, sources, and formation,[5-7] resulting in substantial discrepancies between modeled and measured SOA concentrations.[8, 9] Oxygenated organic molecules (OOMs) are critical intermediates during SOA formation, produced by the oxidation of gaseous precursors such as volatility organic compounds (VOCs).[5, 10] Therefore, the chemical characterization of OOMs is essential to enhance our understanding of the sources, formation pathways, and properties of SOA.[11, 12] However, the identification of atmospheric OOMs at molecular level remains limited, hindering the development of more accurate atmospheric models.

The Tibetan Plateau (TP), often referred to as the “Third Pole”, plays a pivotal role in atmospheric circulation and global climate,[13] while providing substantial water resources to downstream areas.[14] Due to its sparse population and minimal industrial activities, the atmosphere of the TP largely reflects global background conditions.[15] Therefore, climate and cryosphere changes in the TP are particularly sensitive to atmospheric pollutants.[13] As such, it is imperative to assess the extent to which anthropogenic sources impact the TP’s atmosphere. Previous studies using aerosol mass spectrometer (AMS) measurements have demonstrated that secondary formation is a major contributor to OA in the TP. [16-18] However, the specific influence of

anthropogenic sources remains poorly constrained. Shen et al.[19] detected SOA tracers originating from different precursors through offline measurements and found that aromatics may play an important role in SOA formation during certain seasons in the TP. Using a similar approach, Wan et al.[20] identified OA tracers from biomass burning and biogenic sources, while a large unexplained fraction of OA was attributed to other sources, such as anthropogenic emissions. Although offline measurement techniques are effective in identifying SOA tracers from different precursors, the number of detectable compounds is limited, leading to substantial uncertainty into the assessment of anthropogenic contributions. Nitrate chemical ionization mass spectrometry (CIMS) has been employed to measure gas-phase OOMs. Bianchi et al.[21] and Liu et al.[22] revealed the substantial role of biogenic precursors, especially monoterpenes, in SOA formation in the TP. However, nitrate CIMS is more sensitive to highly oxygenated compounds, and molecules with lower oxygen content are often underestimated or even entirely missed.[23] Furthermore, few studies have simultaneously investigated OOMs in both gas and particle phases, which is essential for capturing the full scope of atmospheric oxidation processes and sources contributions. Therefore, a comprehensive chemical characterization of OOMs in both phases is necessary to better quantify the role of anthropogenic sources in shaping the OOMs formation in the TP.

To gain insight into atmospheric gaseous and particulate OOMs in the southeastern TP, we deployed an iodide Chemical Ionization Mass Spectrometry with a Filter Inlet for Gases and AEROsols (FIGAERO-CIMS) at the Lulang observation site, as part of

the @Tibet field campaigns 2021. Iodide CIMS is a powerful tool for measuring OOMs in the atmosphere,[25] exhibiting high selectivity towards highly polarizable compounds.[26] And FIGAERO enables simultaneous gas and particle measurements.[27] Subsequently, we applied a machine learning approach to identify the precursors of the measured OOMs, and elucidated the impacts of anthropogenic sources on gaseous and particulate OOMs in the southeastern TP.

2. MATERIALS AND METHODS

2.1 Measurement Site.

The measurements were conducted at the Lulang observation site (94°44'E, 29°46'N, 3326 m a.s.l.) from April 7 to 24, 2021. Situated in a mountainous valley in the southeastern TP, on the northern bank of the Yarlung Zangbo River,[22] Lulang is characterized by diverse vegetation, including high-altitude forests.[28] A village (Zhaxigang) and a town (Lulang) are located approximately 1.7 km and 4.5 km to the south, respectively. National Road 318 runs east of the site. The site was considered not strongly affected by high-intensity on-road emissions due to few tourist vehicles during the observation period.[29] Overall, it is an ideal location for investigating the impact of anthropogenic sources on the background environments of the TP. Detailed descriptions of this site can be found in previous studies.[22, 28]

2.2 Instrumentation.

An iodide FIGAERO-CIMS (Aerodyne Research Inc.) was deployed to simultaneously measure gaseous and particulate OOMs. The FIGAERO has three

inlet ports that operates in two modes.[27] During the gas mode, ambient air was drawn into the ion molecule reactor (IMR) at a rate of 2 L min^{-1}, where the molecules reacted with iodide ions to form product ions. The pressure and temperature in the IMR were maintained at 200 mbar and 60 ℃, respectively. Concurrently, ambient particles were collected on a PTFE filter (1.0 μm pore size Zefon®, Zefon International) on the FIGAERO at a rate of 6 L min^{-1} to ensure sufficient particle loading (up to 3.6 μg, based on $PM_{2.5}$ measurements).[30] After 20 min in the gas mode, the FIGAERO switched to the particle mode, where particles collected on the filter were thermally desorbed using heated ultrahigh-purity (UHP) N_2 at a rate of 2 L min^{-1}. Then the desorbed vapors were immediately drawn into the IMR for detection. The filter temperature followed a three-step process: ramping from ambient temperature to 180 ℃ over 20 min, soaking at 180 ℃ for 8 min, and cooling back to ambient temperature over 12 min. A complete cycle, including both gas and particle modes, took 1 h.

To quantify the measured OOMs, we calibrated the FIGAERO-CIMS using 9 organic standards. The sensitivity of levoglucosan was applied to all species as the maximum sensitivity of CIMS,[26] thus the reported concentrations represented the lower limits in this study. Considering the lowest sensitivity (Table S1), the concentration of certain OOMs may be underestimated by up to two orders of magnitude. The potential impact of relative humidity on sensitivity was not considered in this study. As the increase of water content may variably affect the sensitivity of OOMs,[25, 31] this simplification could introduce systematic uncertainty into the results. The backgrounds of gas and particle were conducted throughout the

136 measurement period. Peak fitting of the data was processed using the Tofware
137 software (v3.2.2; Tofwerk AG, Switzerland). More details about the FIGAERO-CIMS
138 can be found in Text S1.

139 **2.3 Assigning Precursors to Oxygenated Organic Molecules Using a Machine**
140 **Learning Approach**

141 A detailed workflow to identify the precursors of the measured OOMs is illustrated
142 in Figure S1. OOMs measured by FIGAERO-CIMS originate from both direct
143 emissions and the oxidation of precursors.[31] To assign possible precursors to the
144 measured OOMs, it is necessary to exclude primary OOMs firstly. Biomass burning
145 has been identified as a significant source in the TP.[19, 28] We excluded OOMs likely
146 from biomass burning (BB-OOMs) based on their correlations with $C_6H_{10}O_5$, an
147 important maker for biomass burning.[32] Except for BB-OOMs, most measured OOMs
148 were probably produced through photochemical oxidation, indicated by their higher
149 concentrations during the period from 11:00 to 16:00 (Figure S2), when short-wave
150 radiation was highest.[22] Gas-phase OOMs displayed higher concentration
151 enhancement than particle-phase OOMs, probably due to the mass transfer limitations
152 of gas-particle partitioning.[33] Subsequently, we omitted OOMs with a carbon number
153 $\leq$ 3 (Small OOMs), as these small molecules could derive from the oxidation of
154 multiple precursors.[34, 35]

155 A supervised machine learning approach was used to assign possible precursors to
156 the remaining OOMs based on the methodologies of Qiao et al.[36] and Wang et al.[34] A
157 random forest model was established for classification, requiring a pre-labeled

158 training dataset. Wang et al.[34] has created a dataset comprising known oxidation
159 products from four precursor classes. Since the dataset is concluded from a series of
160 laboratory and field studies using I-CIMS to measure the products of different
161 precursors, it can also be applied in our study. The dataset consists of 82, 126, 215,
162 and 118 products from isoprene, monoterpene, aliphatic, and aromatic, respectively,
163 effectively capturing the characteristics of different precursor classes.[34] The direct
164 application of a multi-class classification model may introduce considerable
165 uncertainty due to the presence of OOMs that originate from multiple precursors. To
166 overcome this issue, we reformulated the original four-class classification task into
167 four independent binary classification tasks. In each task, a separate random forest
168 model was trained to predict whether a given OOM belongs to the corresponding
169 precursor class or not. This approach allows for overlapping classifications and
170 improves the robustness of precursor attribution. Model input features included the
171 number of carbon, hydrogen, oxygen, and nitrogen atoms (n_C, n_H, n_O, and n_N,
172 respectively), as well as calculated parameters such as double bond equivalent (DBE),
173 hydrogen-to-carbon ratio (H/C), oxygen-to-carbon ratio (O/C), and average carbon
174 oxidation state ($\overline{OS}_C$). The random forest model was implemented using the sklearn
175 package (v1.3.0) in Python, producing the occurrence probability for each OOM
176 across the four precursor classes. We replaced the probability ≤ 0.6 with 0, proposing
177 that the OOM unlikely came from the corresponding precursor. Then the signal of
178 each OOM was assigned to four precursor classes based on the ratio of occurrence
179 probabilities. If no probability was > 0.6, the OOM was labeled as “Other OOMs”.

More details about the probability calculations can be found in Text S2.

To train and evaluate the random forest model, the dataset was divided into two subsets randomly: 70% for training and 30% for testing. We employed a grid search method to determine optimal model parameters. Three parameters were examined in our study, i.e. the number of trees (from 1 to 150), the maximum depth of each tree (from 1 to 14), and the max features for the best split at each node of a decision tree (from 1 to 8). Model performance was assessed using three metrics, i.e. *Precision, Recall, and F1-score* (the calculation detailed in Text S3). The variation of the metrics with three selected parameters was explored, as shown in Figure S3. The optimal value was 21, 8, and 2 for the number of trees, the maximum depth of each tree, and the max features, respectively. *Precision, Recall, and F1-score* of final random forest model was calculated using these optimal values, as listed in Table S2. All *F1-scores* were ≥ 0.75, indicating high accuracy in predicting the precursors for OOMs. In addition, a 5-fold cross-validation was conducted to prevent overfitting (Text S4 and Figure S4), with the average *F1-score* of four precursor classes at each iteration > 0.75, thus demonstrating model reliability.

3. RESULTS AND DISCUSSION

3.1 Characteristics of Oxygenated Organic Molecules in the Ambient Air of Tibet

A total of 653 OOMs were identified within the m/z 150-400 Th in this study, including 347 organic carbon species (OC = $C_xH_yO_z$, where $1 \leq x \leq 20$, y is an even number not exceeding 2x+2, and $z \geq 2$) and 306 organic nitrate species (ON =

$C_xH_yO_zN_{1\ or\ 2,}$ when N_1, $1 \leq x \leq 20$, y is an odd number not exceeding 2x+1, and $z \geq 2$; when N_2, $1 \leq x \leq 20$, y is an even number not exceeding 2x, and $z \geq 4$). The campaign-averaged mass spectra of the measured gaseous and particulate OOMs are shown in Figure S5. In general, larger OOMs exhibited a higher proportion in the particle phase compared to the gas phase. The signal fractions decreased with the increase of m/z when m/z was > 290 Th in the gas phase. The signal-weighted average formulas of gaseous and particulate OOMs were $C_{5.1}H_{7.7}O_{3.8}N_{0.2}$ and $C_{6.8}H_{9.3}O_{4.7}N_{0.3}$, corresponding to molecular weights of 132 and 171 g mol^{-1}, respectively. The oxygen number was higher, while the O/C was lower in the particle phase than those in the gas phase, attributed to the larger fractions of more oxidized small OOMs in the gas phase. It should be noted that several small OOMs exhibited high abundances in the particle phase, likely resulting from thermal decomposition of larger OOMs during thermal desorption on FIGAERO.[27, 37] The presence of small OOMs could lead to an underestimation of effective molecular weight and an overestimation of bulk volatility in the particle phase. Organic nitrates were clearly observed in both gas and particle phases, indicating the significant role of NO_x (3.7 ± 2.4 ppbv during the observation period) in local atmospheric chemistry. It should be noted that in addition to anthropogenic sources, NO_x may also come from strong natural sources in the TP, such as soil microbial activity, lakes, and lightning-induced NO_x.[38, 39]

The numbers of carbon and oxygen of the measured gaseous and particulate OOMs were analyzed, as shown in Figure 1. $C_{1\text{-}2}$ OOMs constituted a significant proportion

(27.4%) in the gas phase, especially CH_2O_2 (16.0%). CH_2O_2 has been assigned as formic acid, commonly found in various atmospheres and produced by various precursors.[40] Apart from $C_{1\text{-}2}$ OOMs, $C_{4\text{-}7}$ OOMs were the main components in the gas phase, accounting for 44.8% of the total measured OOMs. In contrast, besides $C_{5\text{-}7}$ OOMs, $C_{8\text{-}10}$ OOMs also exhibited high abundances in the particle phase, with the total proportion of 26.2%. The major oxygen number was 4 in both gas and particle phases, comprising 28.5% and 18.8%, respectively. Notably, the fraction of highly oxygenated organic molecules ($n_O \geq 6$) was significantly higher in the particle phase than that in the gas phase.

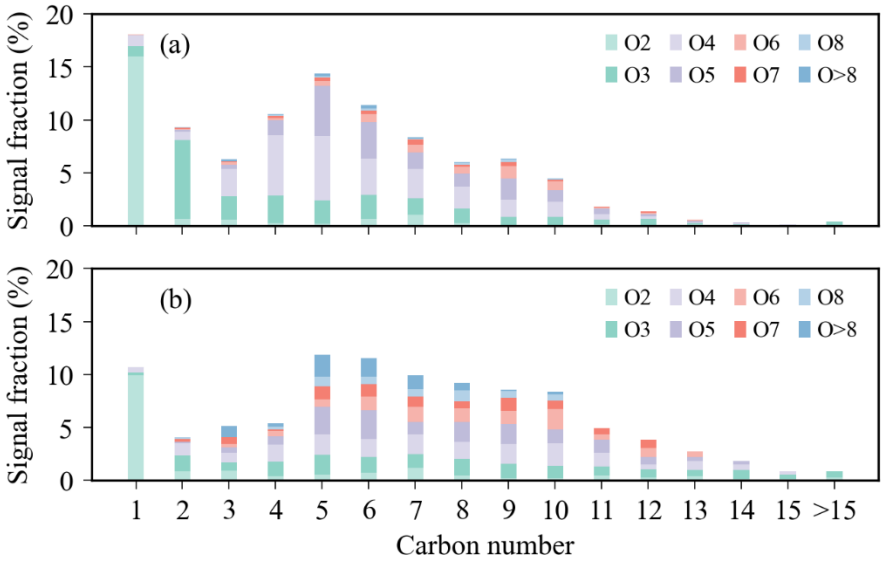

Figure 1. The distributions of carbon and oxygen numbers of the measured OOMs. (a) Gas phase; (b) Particle phase.

The different distribution characteristics between gaseous and particulate OOMs depend on their different partition coefficients, which are affected by volatilities and functional groups.[41] Therefore, this study investigated the relationship between $\overline{OS}_C$

and saturation concentration (C^*) of measured OOMs, representing oxidation degree and volatility, respectively, as shown in Figure 2. The calculations of $\overline{OS}_C$ and C^* can be found in Text S5. Several OOMs appeared with high volatility and oxidation degree in both gas and particle phases, probably resulting from fragmentation reactions during sufficient oxidation.[41] Except for these OOMs, $\overline{OS}_C$ generally increased with the decrease of $\log_{10}C^*$, indicating that the addition of oxygen-containing functional groups reduced volatility.[41] OOMs with lower volatilities were more likely to partition into the particle phase, demonstrated by their higher F_p (the ratio of concentration in the particle phase to the sum concentration in both the gas and particle phases) (Figure S6). However, some compounds with high volatility also exhibited high F_p, probably due to the decomposition on FIGAERO.[27, 37] The relationship of F_p and $\log_{10}C^*$ had a systematic shift from the theoretical line based on gas-particle partitioning, indicating the volatility might be overestimated through the formula method in our study.[37] On the contrary, there is no obvious correlation between F_p and $\overline{OS}_C$. Gaseous OOMs predominantly fell within the intermediate volatility organic compounds (IVOCs) range, accounting for 67.2% of the total measured OOMs. While particulate OOMs were mainly distributed across both IVOCs and semi-volatile organic compounds (SVOCs) ranges, accounting for 43.5% and 33.5%, respectively.

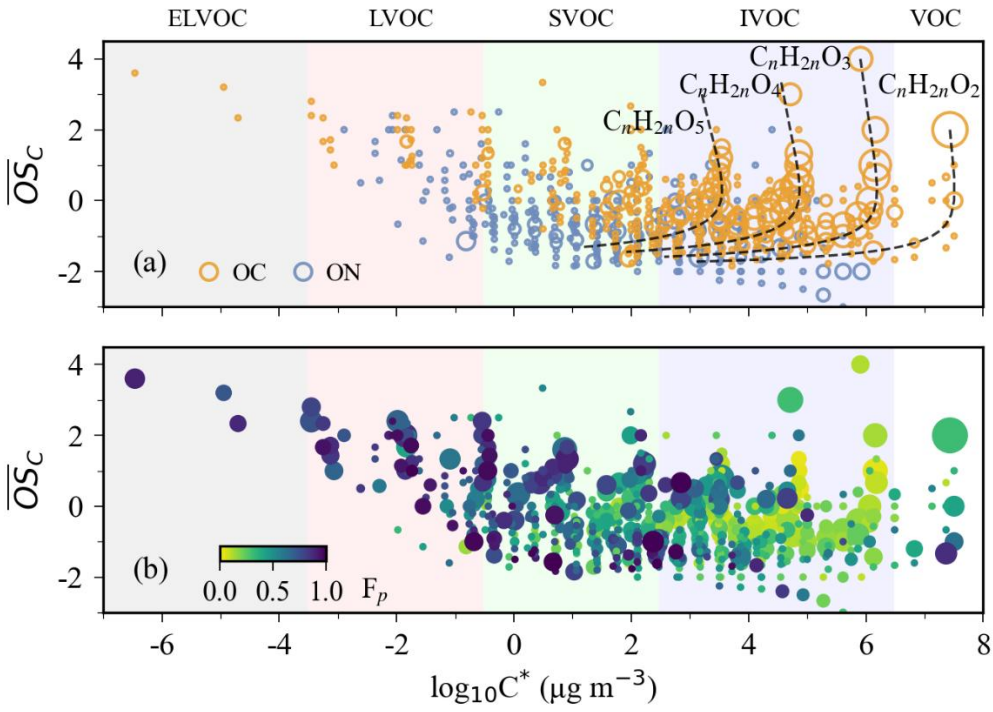

Figure 2. Relationship between average carbon oxidation state ($\overline{OS}_C$) and logarithmic saturated vapor concentration ($\log_{10}C^*$) of the measured OOMs. (a) Gas phase; (b) Particle phase. The circle size is proportional to the logarithmic signal fraction. The black dotted lines in panel (a) are theoretical curves for these formulas. The circles in panel (b) are colored by F_p (the ratio of concentration in the particle phase to the sum concentration in the gas and particle phases). Both (a) and (b) include all measured OC and ON species.

3.2 Precursor Apportionment of Oxygenated Organic Molecules

Biomass burning has been recognized as an important source in the TP.[28] $C_6H_{10}O_5$ detected by FIGAERO-CIMS has been previously attributed to levoglucosan and its isomers,[31, 42] regarded as important makers for biomass burning.[32] The average mass concentration of particulate $C_6H_{10}O_5$ was 1.21 ± 1.91 ng m^{-3} in this study, slightly

lower than the result at another site in the TP,[19] but significantly lower by 1-2 orders of magnitude compared to the results from typical megacities.[11, 31] This may be attributed to the enhanced intensity of biomass burning activities and unfavorable meteorological conditions during certain seasons in megacities.[11, 43] The diurnal profile of both gaseous and particulate $C_6H_{10}O_5$ exhibited a significant peak in the morning (Figure S7), suggesting enhanced biomass burning activity. In addition, $C_6H_5NO_4$, $C_5H_{10}O_4$, and $C_8H_{12}O_6$ displayed strong correlations with $C_6H_{10}O_5$ in both gas and particle phases ($R > 0.8$), indicating that they might also originate from biomass burning.

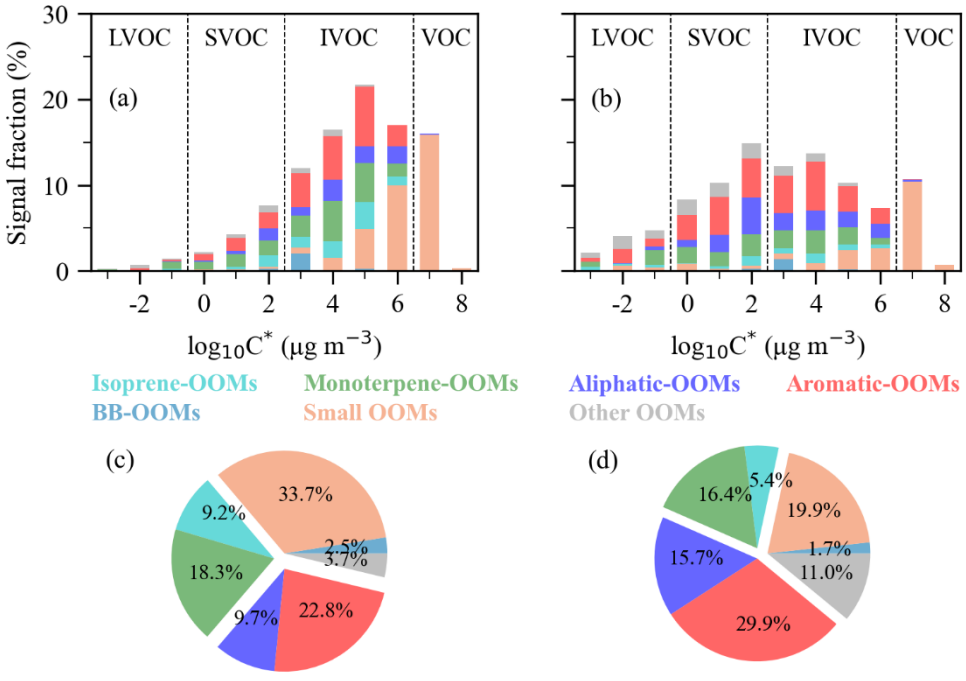

Figure 3. Contributions of different precursor classes to the measured OOMs. Contributions of different OOMs at each volatility bin in the (a) gas phase, and (b) particle phase, respectively. Contributions of different OOMs to the total

measured OOMs in the (c) gas phase, and (d) particle phase, respectively. "BB-OOMs" represents the OOMs from biomass burning. "Small OOMs" represents the OOMs with carbon number ≤ 3.

After excluding 4 BB-OOMs and 61 small OOMs, we identified 50 isoprene-OOMs, 142 monoterpene-OOMs, 157 aliphatic-OOMs, 228 aromatic-OOMs, and 89 aromatic-OOMs using the random forest model (Figure 3 and Figure S8). And the remaining 89 OOMs were classified into "Other OOMs". The diurnal patterns of four types of OOMs are shown in Figure S9. As mentioned above, $C_{1\text{-}3}$ OOMs were excluded as small OOMs from classification, due to the large overlap of them in the oxidation products of various precursors.[34] Gaseous and particulate BB-OOMs accounted for only 2.5% and 1.7% of the total measured OOMs, respectively. As mentioned in the method, BB-OOMs only represent the compounds directly emitted from biomass burning. Chen et al. [28]revealed the important contribution of biomass burning to particles at the same site through the measurements of n-alkanes and polycyclic aromatic hydrocarbons, which cannot be measured by FIGAERO-CIMS. The measured oxidation products of n-alkanes and polycyclic aromatic hydrocarbons, which may be emitted by biomass burning, will be categorized as aliphatic-OOMs and aromatic-OOMs, respectively, in our study. As shown in Figure S10, over 75% of isoprene-OOMs, aliphatic-OOMs, and aromatic-OOMs were distributed in the IVOCs range in the gas phase. While 71.9% and 23.1% of gaseous monoterpene-OOMs were distributed in the IVOCs and SVOCs ranges, respectively. In contrast, more isoprene-OOMs, monoterpene-OOMs, aliphatic-OOMs, and aromatic-OOMs were

found in the SVOCs range in the particle phase, indicating that these OOMs were more likely to partition into particle. Wang et al. (2024)[34] showed that the OOMs derived from four precursors mainly distributed in the low volatility organic compounds (LVOCs) range at multiple sites. This is because the volatility estimated through formula method in our study would be several orders of magnitude higher than that estimated through thermogram method in Wang et al. (2024).[37] To investigate the sources of OOMs from different precursors, we simply assumed that isoprene-OOMs and monoterpene-OOMs originated from biogenic sources, and aliphatic-OOMs and aromatic-OOMs originated from anthropogenic sources.[35] Isoprene may be emitted from anthropogenic sources, but in background region the anthropogenic fraction of isoprene is quite small.[45] Aromatics can also come from biogenic sources, such as cyanobacteria in the lake.[46] Since there are no large lakes around the sampling site, this impact can also be ignored. BB-OOMs were not categorized as biogenic or anthropogenic sources. Due to the small fraction of BB-OOMs, it will not significantly affect the conclusions. Monoterpene-OOMs and isoprene-OOMs constituted only 27.5% and 21.8% of the total measured OOMs in the gas and particle phases, respectively. The contribution of monoterpene-OOMs was significantly higher than that of isoprene-OOMs, indicating that monoterpenes might be more important in biogenic SOA formation in the southeastern TP. Aliphatic-OOMs contributed 9.7% and 15.7% to the total measured OOMs in the gas and particle phases, respectively, with alkanes regarded as the dominant precursors.[35] The proportions of aromatic-OOMs were 22.8% and 29.9%, respectively.

Aliphatic-OOMs and aromatic-OOMs contributed 32.5% and 45.6% to the total measured OOMs in the gas and particle phases, respectively, emphasizing a more critical role of anthropogenic sources in OOMs formation than biogenic sources in the southeastern TP. If all other OOMs were classified as biogenic OOMs, the fraction of total biogenic OOMs would be 31.2% and 32.8% in the gas and particle phases, respectively, still lower than that of anthropogenic OOMs, indicating these unclassified OOMs would not significantly impact the conclusions. Since small OOMs account for only a minor fraction in the particle phase, including them in the model did not significantly affect the overall conclusions (Figure S11). However, the contribution of biogenic sources to OOMs would increase to a level comparable to that of anthropogenic sources, as a larger number of small OOMs were classified as biogenic OOMs. This highlights the need for accurate source apportionment of small OOMs in future studies, for example through isotopic analysis.[44]

To investigate the impact of regional transport to OOMs formation, a cluster analysis of 72h backward air mass trajectories at 500m above ground level was performed, as shown in Figure S12. This height was chosen to better represent the lower free troposphere over the plateau's complex terrain, such as mountain and valley.[38] The 72h duration was chosen based on the typical atmospheric lifetime of OOMs. The air masses over the Lulang site primarily originated from the south, with the shortest transport distance constituting 81% of all trajectories, indicating that local emissions likely played a dominant role in shaping the observed OOMs composition. There are no significant differences in OOMs compositions in both gas and particle

phases among different clusters, as shown in Figure S13. Although the air mass clusters varied in transport distance, they all passed through the region associated with the dominant short-range cluster. Consequently, characteristics of OOMs from long-range transport may be masked by local emissions. Given the proximity of a village, a town, and National Road 318, anthropogenic precursors and their oxidation products may be transported to the Lulang site by these prevailing air masses from the three nearby emission regions.

To the best of our knowledge, the present work is the first study to assign specific precursors to OOMs measured by FIGAERO-CIMS in the TP. Previous studies have resolved the contributions of primary and secondary sources to OA in other TP regions, but the roles of different precursors have not been well characterized.[16, 17, 47] Through the measurement of SOA tracers, Shen et al.[19] found that secondary organic carbons (SOC) from aromatics accounted for approximately 25% of the total estimated SOC at Nam Co lake. Guo et al.[29] demonstrated the significant contributions of aromatics to SOA through the estimation of SOA potentials of VOC components at the same site. However, Liu et al.[22] reported that anthropogenic precursors explained only 10% of extremely low-volatility organic compounds measured by nitrate CIMS at the same site, lower than our results. The difference may be attributed to the different measurement ranges of organic compounds,[48] as FIGAERO-CIMS mainly measured S/IVOCs in our study. The accurate quantification of both instruments may be important for their comparability in future study.[49] It should be noted that the relative contributions of anthropogenic and biogenic sources

375 to OOMs in the TP can be influenced by multiple factors, such as emissions patterns,
376 atmospheric conditions, and sampling period. Bianchi et al.[21] reported that biogenic
377 sources were an important contributor to particle at a site located at 5079 m a.s.l.,
378 possibly due to lower anthropogenic emissions in that region. Shen et al.[19] found that
379 the contribution of anthropogenic sources to SOC increased significantly in April
380 compared to other summer months, which coincides with the sampling period of this
381 study. In addition, the impacts of anthropogenic sources on atmospheric species have
382 also been observed at other mountain sites.[50-52] For instance, Zhang et al.[53] discovered
383 that anthropogenic sources contributed 16%-35% to total gaseous organic compounds
384 at Shanghuang Mountain. Therefore, establishing the links between precursors and
385 OOMs in background sites should be given more consideration in future studies for
386 better understanding the impacts of anthropogenic sources on background
387 atmosphere.

388 Although our study provides valuable insight into the OOMs species in the TP,
389 there are several limitations that need to be considered. Firstly, the sampling duration
390 is limited to approximately two weeks in April 2021. As stated by previous studies,[19,
391 28] the emissions of biogenic and anthropogenic sources display significant seasonal
392 variation in the TP. For instance, biogenic emissions are typically enhanced during
393 summer,[19] while anthropogenic emissions associated with tourism may peak at other
394 seasons.[28] The relative importance of biogenic and anthropogenic sources may vary in
395 different seasons. Nevertheless, our results provide a representative snapshot of
396 OOMs characteristics during the spring period in the TP and can serve as a baseline

for future seasonal comparisons. Secondly, there exist some uncertainties of classifications based on the machine learning approach, especially for those OOMs from multiple precursors. There are 18 species belonging to both isoprene-OOMs and aliphatic-OOMs, and 29 species belonging to both monoterpene-OOMs and aromatic-OOMs in the dataset.[34] We compared the occurrence probability of these OOMs, as shown in Figure S14. The probability of aromatic was higher than that of monoterpene for most OOMs derived from both aromatic and monoterpene, indicating the aromatic-OOMs would be overestimated in the actual atmosphere. In the real atmosphere, the contributions of different sources to these overlapping OOMs may be influenced by meteorological conditions and the relative proportions of emission sources. However, these factors are not considered in the current model. To better understand this uncertainty, we performed a sensitivity analysis on the model. We considered two scenarios: all overlapping OOMs were assumed to originate from anthropogenic sources, and all overlapping OOMs were assumed to originate from biogenic sources. The results (Figure S11) showed that anthropogenic OOMs remained more abundant than biogenic OOMs, except for the gas phase under the second scenario. This indicates that the classification of gas-phase OOMs may be more susceptible to uncertainties associated with overlapping OOMs. In addition, the value of threshold (0.6) may affect the probabilities of overlapping OOMs. To assess the sensitivity of our results to this parameter, we also examined thresholds of 0.4 and 0.8, with the results shown in Figure S11. In both cases, contributions of anthropogenic sources remained higher than those of biogenic sources, suggesting the

robustness of the results with respect to the choice of threshold. Thirdly, considering the same sensitivity was assumed for all measured OOMs, the contribution of different sources has large uncertainty. The transmission, which is a function of m/z, is an important factor in affecting the sensitivity of different OOMs.[54] The distributions of biogenic and anthropogenic OOMs on m/z were compared, as shown in Figure S15. In the gas phase, their distributions were similar, indicating the transmission has little impact on the contribution of two sources. In the particle phase, biogenic OOMs distributed more in the large m/z range, indicating its contribution would be slightly underestimated.

3.3 Atmospheric Implications

As the "Third Pole", the TP significantly affects atmospheric circulation, global climate, and cryosphere change.[13] The TP's atmospheric environment has been considered representative of global background conditions due to limited human activities.[15] However, economic development has resulted in the inevitable emission of anthropogenic pollutants into the TP's environments.[55, 56] Kang et al.[13] noted that these exogenous pollutants substantially impact regional climate and environmental changes in the TP. In recent decades, the TP has experienced considerable climate warming.[57] Anthropogenic pollutants can contribute to climate change through their effects on solar radiation.[58] Our study highlights the significant impacts of anthropogenic sources on OOMs formation in the southeastern TP, with aromatic-OOMs being the dominant components of particulate OOMs. Laboratory

investigation by Nakayama et al.[59] demonstrated that secondary organic aerosols from toluene photooxidation exhibit substantial light absorption properties, indicating substantial brown carbon formation that contributes to positive radiative forcing and atmospheric warming. These experimentally determined optical properties are applicable to our observed anthropogenic OOMs, as aromatic precursors may undergo comparable photooxidation.[60] Ji et al.[58] conducted comprehensive simulations of carbonaceous aerosols over the TP and adjacent regions, revealing the importance of aerosol longwave radiative forcing to climatic effect of aerosols. Our molecular-level characterization of anthropogenic OOMs provides crucial chemical speciation data that bridges the gap between emission sources and the formation of climatically active light-absorbing secondary organic compounds, thereby enabling more accurate parameterization of aerosol optical properties in regional climate models. These findings underscore the necessity of considering anthropogenic influences in future research. Overall, our study provides valuable insights into atmospheric species, and enhances our understanding of pollutant sources and atmospheric chemical processes in the TP.

Supporting information

Details about the FIGAERO-CIMS (Text S1, and Table S1). Details about the random forest approach (Text S2-S4, Table S2, Figure S1, S3, S4, and S14). Calculations of C^* and $\overline{OS}_C$ (Text S5). Ratio of average concentrations between two different periods (Figure S2). Campaign-averaged mass spectra (Figure S5). Relationship of F_p with

463 $\log_{10}C^*$ and $\overline{OS}_C$ (Figure S6). Diurnal variations of BB-OOMs (Figure S7).
464 Classification of the measured OOMs (Figure S8, S9, and S10). Sensitivity analysis
465 (Figure S11). Cluster results of backward trajectories (Figure S12 and S13).
466 Distribution of different OOMs on m/z (Figure S15).
467

468 ## Conflict of Interest Disclosure

469 The authors declare no competing financial interest.
470

471 ## Acknowledgment

472 This research was supported by the National Key R&D Program of China
473 (2022YFC3701000, Task 2), National Natural Science Foundation of China-Creative
474 Research Group Fund (2222100), National Natural Science Foundation of China
475 (42175120), special fund of State Key Joint Laboratory of Environmental Simulation
476 and Pollution Control (24Y01ESPCP).
477

478 ## Reference

479 (1) Jimenez, J. L.; Canagaratna, M. R.; Donahue, N. M.; Prevot, A. S. H.; Zhang, Q.; Kroll, J.
480 H.; DeCarlo, P. F.; Allan, J. D.; Coe, H.; Ng, N. L.; et al. Evolution of organic aerosols in the
481 atmosphere. *Science* **2009**, *326* (5959), 1525-1529. DOI: 10.1126/science.1180353.
482 (2) Guo, S.; Hu, M.; Zamora, M. L.; Peng, J. F.; Shang, D. J.; Zheng, J.; Du, Z. F.; Wu, Z.;
483 Shao, M.; Zeng, L. M.; et al. Elucidating severe urban haze formation in China. *P Natl Acad*
484 *Sci USA* **2014**, *111* (49), 17373-17378. DOI: 10.1073/pnas.1419604111.
485 (3) D'Andrea, S. D.; Hakkinen, S. A. K.; Westervelt, D. M.; Kuang, C.; Levin, E. J. T.;
486 Kanawade, V. P.; Leaitch, W. R.; Spracklen, D. V.; Riipinen, I.; Pierce, J. R. Understanding

global secondary organic aerosol amount and size-resolved condensational behavior. *Atmospheric Chemistry and Physics* **2013**, *13* (22), 11519-11534. DOI: 10.5194/acp-13-11519-2013.

(4) Pye, H. O. T.; Ward-Caviness, C. K.; Murphy, B.; Appel, K. W.; Seltzer, K. M. Secondary organic aerosol association with cardiorespiratory disease mortality in the United States. *Nature Communications* **2021**, *12* (1), s41467-41021-27484-41461. DOI: ARTN 721510.1038/s41467-021-27484-1.

(5) Hallquist, M.; Wenger, J. C.; Baltensperger, U.; Rudich, Y.; Simpson, D.; Claeys, M.; Dommen, J.; Donahue, N. M.; George, C.; Goldstein, A. H.; et al. The formation, properties and impact of secondary organic aerosol: Current and emerging issues. *Atmospheric Chemistry and Physics* **2009**, *9* (14), 5155-5236. DOI: DOI 10.5194/acp-9-5155-2009.

(6) Srivastava, D.; Vu, T. V.; Tong, S. R.; Shi, Z. B.; Harrison, R. M. Formation of secondary organic aerosols from anthropogenic precursors in laboratory studies. *Npj Clim Atmos Sci* **2022**, *5* (1), s41612-41022-00238-41616. DOI: ARTN 2210.1038/s41612-022-00238-6.

(7) Guo, S.; Hu, M.; Peng, J. F.; Wu, Z. J.; Zamora, M. L.; Shang, D. J.; Du, Z. F.; Zheng, J.; Fang, X.; Tang, R. Z.; et al. Remarkable nucleation and growth of ultrafine particles from vehicular exhaust. *P Natl Acad Sci USA* **2020**, *117* (7), 3427-3432. DOI: 10.1073/pnas.1916366117.

(8) Li, J. Y.; Zhang, H. W.; Li, L.; Ye, F.; Wang, H. L.; Guo, S.; Zhang, N.; Qin, M. M.; Hu, J. L. Modeling Secondary Organic Aerosols in China: State of the Art and Perspectives. *Curr Pollut Rep* **2023**, *9* (1), 22-45. DOI: 10.1007/s40726-022-00246-3.

(9) Yu, Y.; Wang, H.; Wang, T. T.; Song, K.; Tan, T. Y.; Wan, Z. C.; Gao, Y. Q.; Dong, H. B.; Chen, S. Y.; Zeng, L. M.; et al. Elucidating the importance of semi-volatile organic compounds to secondary organic aerosol formation at a regional site during the EXPLORE-YRD campaign. *Atmospheric Environment* **2021**, *246*, 118043. DOI: ARTN 11804310.1016/j.atmosenv.2020.118043.

(10) Bianchi, F.; Kurtén, T.; Riva, M.; Mohr, C.; Rissanen, M. P.; Roldin, P.; Berndt, T.; Crounse, J. D.; Wennberg, P. O.; Mentel, T. F.; et al. Highly oxygenated organic molecules (HOM) from gas-phase autoxidation involving peroxy radicals: A key contributor to

516 atmospheric aerosol. *Chem Rev* **2019**, *119* (6), 3472-3509. DOI:
517 10.1021/acs.chemrev.8b00395.
518 (11) Zheng, Y.; Chen, Q.; Cheng, X.; Mohr, C.; Cai, J.; Huang, W.; Shrivastava, M.; Ye, P.; Fu,
519 P.; Shi, X.; et al. Precursors and pathways leading to enhanced secondary organic aerosol
520 formation during severe haze episodes. *Environmental Science & Technology* **2021**, *55* (23),
521 15680-15693. DOI: 10.1021/acs.est.1c04255.
522 (12) Ye, C.; Liu, Y.; Yuan, B.; Wang, Z.; Lin, Y.; Hu, W.; Chen, W.; Li, T.; Song, W.; Wang, X.;
523 et al. Low-NO-like Oxidation Pathway Makes a Significant Contribution to Secondary
524 Organic Aerosol in Polluted Urban Air. *Environmental Science & Technology* **2023**, *57* (37),
525 13912-13924. DOI: 10.1021/acs.est.3c01055.
526 (13) Kang, S.; Zhang, Q.; Qian, Y.; Ji, Z.; Li, C.; Cong, Z.; Zhang, Y.; Guo, J.; Du, W.; Huang,
527 J.; et al. Linking atmospheric pollution to cryospheric change in the Third Pole region: current
528 progress and future prospects. *Natl Sci Rev* **2019**, *6* (4), 796-809. DOI: 10.1093/nsr/nwz031.
529 (14) Immerzeel, W. W.; van Beek, L. P. H.; Bierkens, M. F. P. Climate Change Will Affect the
530 Asian Water Towers. *Science* **2010**, *328* (5984), 1382-1385. DOI: 10.1126/science.1183188.
531 (15) Wang, Y. S.; Xin, J. Y.; Li, Z. Q.; Wang, S. G.; Wang, P. C.; Hao, W. M.; Nordgren, B. L.;
532 Chen, H. B.; Wang, L. L.; Sun, Y. Seasonal variations in aerosol optical properties over China.
533 *J Geophys Res-Atmos* **2011**, *116*. DOI: Artn D1820910.1029/2010jd015376.
534 (16) Xu, J.; Zhang, Q.; Shi, J.; Ge, X.; Xie, C.; Wang, J.; Kang, S.; Zhang, R.; Wang, Y.
535 Chemical characteristics of submicron particles at the central Tibetan Plateau: insights from
536 aerosol mass spectrometry. *Atmospheric Chemistry and Physics* **2018**, *18* (1), 427-443. DOI:
537 10.5194/acp-18-427-2018.
538 (17) Zhang, X.; Xu, J.; Kang, S.; Zhang, Q.; Sun, J. Chemical characterization and sources of
539 submicron aerosols in the northeastern Qinghai–Tibet Plateau: insights from high-resolution
540 mass spectrometry. *Atmospheric Chemistry and Physics* **2019**, *19* (11), 7897-7911. DOI:
541 10.5194/acp-19-7897-2019.
542 (18) Du, W.; Sun, Y. L.; Xu, Y. S.; Jiang, Q.; Wang, Q. Q.; Yang, W.; Wang, F.; Bai, Z. P.;
543 Zhao, X. D.; Yang, Y. C. Chemical characterization of submicron aerosol and particle growth
544 events at a national background site (3295 m a.s.l.) on the Tibetan Plateau. *Atmospheric*

Chemistry and Physics **2015**, *15* (18), 10811-10824. DOI: 10.5194/acp-15-10811-2015.

(19) Shen, R. Q.; Ding, X.; He, Q. F.; Cong, Z. Y.; Yu, Q. Q.; Wang, X. M. Seasonal variation of secondary organic aerosol tracers in Central Tibetan Plateau. *Atmospheric Chemistry and Physics* **2015**, *15* (15), 8781-8793. DOI: 10.5194/acp-15-8781-2015.

(20) Wan, X.; Fu, P.; Kang, S.; Kawamura, K.; Wu, G.; Li, Q.; Gao, S.; Cong, Z. Organic aerosols in the inland Tibetan Plateau: New insights from molecular tracers. *Science of The Total Environment* **2023**, *884*. DOI: 10.1016/j.scitotenv.2023.163797.

(21) Bianchi, F.; Junninen, H.; Bigi, A.; Sinclair, V. A.; Dada, L.; Hoyle, C. R.; Zha, Q.; Yao, L.; Ahonen, L. R.; Bonasoni, P.; et al. Biogenic particles formed in the Himalaya as an important source of free tropospheric aerosols. *Nature Geoscience* **2020**, *14* (1), 4-9. DOI: 10.1038/s41561-020-00661-5.

(22) Liu, Y.; Nie, W.; Qi, X.; Li, Y.; Xu, T.; Liu, C.; Ge, D.; Chen, L.; Niu, G.; Wang, J.; et al. The Pivotal Role of Heavy Terpenes and Anthropogenic Interactions in New Particle Formation on the Southeastern Qinghai-Tibet Plateau. *Environmental Science & Technology* **2024**. DOI: 10.1021/acs.est.4c04112.

(23) Riva, M.; Rantala, P.; Krechmer, J. E.; Peräkylä, O.; Zhang, Y.; Heikkinen, L.; Garmash, O.; Yan, C.; Kulmala, M.; Worsnop, D.; Ehn, M. Evaluating the performance of five different chemical ionization techniques for detecting gaseous oxygenated organic species. *Atmospheric Measurement Techniques* **2019**, *12* (4), 2403-2421. DOI: 10.5194/amt-12-2403-2019.

(24) An, Y.; Xu, J.; Feng, L.; Zhang, X.; Liu, Y.; Kang, S.; Jiang, B.; Liao, Y. Molecular characterization of organic aerosol in the Himalayas: insight from ultra-high-resolution mass spectrometry. *Atmospheric Chemistry and Physics* **2019**, *19* (2), 1115-1128. DOI: 10.5194/acp-19-1115-2019.

(25) Lee, B. H.; Lopez-Hilfiker, F. D.; Mohr, C.; Kurtén, T.; Worsnop, D. R.; Thornton, J. A. An iodide-adduct high-resolution time-of-flight chemical-ionization mass spectrometer: Application to atmospheric inorganic and organic compounds. *Environmental Science & Technology* **2014**, *48* (11), 6309-6317. DOI: 10.1021/es500362a.

(26) Iyer, S.; Lopez-Hilfiker, F.; Lee, B. H.; Thornton, J. A.; Kurtén, T. Modeling the

574 detection of organic and inorganic compounds using iodide-based chemical ionization. *The*
575 *Journal of Physical Chemistry A* **2016**, *120* (4), 576-587. DOI: 10.1021/acs.jpca.5b09837.
576 (27) Lopez-Hilfiker, F. D.; Mohr, C.; Ehn, M.; Rubach, F.; Kleist, E.; Wildt, J.; Mentel, T. F.;
577 Lutz, A.; Hallquist, M.; Worsnop, D.; Thornton, J. A. A novel method for online analysis of
578 gas and particle composition: Description and evaluation of a Filter Inlet for Gases and
579 AEROsols (FIGAERO). *Atmospheric Measurement Techniques* **2014**, *7* (4), 983-1001. DOI:
580 10.5194/amt-7-983-2014.
581 (28) Chen, Y.; Cao, J.; Zhao, J.; Xu, H.; Arimoto, R.; Wang, G.; Han, Y.; Shen, Z.; Li, G.
582 n-Alkanes and polycyclic aromatic hydrocarbons in total suspended particulates from the
583 southeastern Tibetan Plateau: Concentrations, seasonal variations, and sources. *Science of The*
584 *Total Environment* **2014**, *470-471*, 9-18. DOI: 10.1016/j.scitotenv.2013.09.033.
585 (29) Guo, S.; Ye, C.; Lin, W.; Chen, Y.; Zeng, L.; Yu, X.; Cui, J.; Zhang, C. Volatile organic
586 compounds at a highland forest site in the southeast of the Tibetan Plateau: Source
587 apportionment and reactivity contributions. *Environ Pollut* **2025**, *366*. DOI:
588 10.1016/j.envpol.2024.125410.
589 (30) Wang, J.; Wang, J.; Zhang, Y.; Liu, T.; Chi, X.; Huang, X.; Ge, D.; Lai, S.; Zhu, C.; Wang,
590 L.; et al. Impacts of elevated anthropogenic emissions on physicochemical characteristics of
591 black-carbon-containing particles over the Tibetan Plateau. *Atmospheric Chemistry and*
592 *Physics* **2024**, *24* (19), 11063-11080. DOI: 10.5194/acp-24-11063-2024.
593 (31) Ye, C.; Yuan, B.; Lin, Y.; Wang, Z.; Hu, W.; Li, T.; Chen, W.; Wu, C.; Wang, C.; Huang,
594 S.; et al. Chemical characterization of oxygenated organic compounds in the gas phase and
595 particle phase using iodide CIMS with FIGAERO in urban air. *Atmospheric Chemistry and*
596 *Physics* **2021**, *21* (11), 8455-8478. DOI: 10.5194/acp-21-8455-2021.
597 (32) Bhattarai, H.; Saikawa, E.; Wan, X.; Zhu, H. X.; Ram, K.; Gao, S. P.; Kang, S. C.; Zhang,
598 Q. G.; Zhang, Y. L.; Wu, G. M.; et al. Levoglucosan as a tracer of biomass burning: Recent
599 progress and perspectives. *Atmos Res* **2019**, *220*, 20-33. DOI:
600 10.1016/j.atmosres.2019.01.004.
601 (33) Lutz, A.; Mohr, C.; Le Breton, M.; Lopez-Hilfiker, F. D.; Priestley, M.; Thornton, J. A.;
602 Hallquist, M. Gas to Particle Partitioning of Organic Acids in the Boreal Atmosphere. *ACS*

603 *Earth and Space Chemistry* **2019**, *3* (7), 1279-1287. DOI:
604 10.1021/acsearthspacechem.9b00041.
605 (34) Wang, X.; Zhao, Y.; Hu, K.; Wang, J.; Wang, Q.; Chen, N.; Zhu, B.; Zhang, H.-H.; Yu, H.
606 Linking Precursors and Volatility of Ambient Oxygenated Organic Aerosols Using Thermal
607 Desorption Measurement and Machine Learning. *ACS ES&T Air* **2024**. DOI:
608 10.1021/acsestair.4c00076.
609 (35) Nie, W.; Yan, C.; Huang, D. D.; Wang, Z.; Liu, Y.; Qiao, X.; Guo, Y.; Tian, L.; Zheng, P.;
610 Xu, Z.; et al. Secondary organic aerosol formed by condensing anthropogenic vapours over
611 China's megacities. *Nature Geoscience* **2022**, *15* (4), 255-261. DOI:
612 10.1038/s41561-022-00922-5.
613 (36) Qiao, X.; Li, X.; Yan, C.; Sarnela, N.; Yin, R.; Guo, Y.; Yao, L.; Nie, W.; Huang, D.;
614 Wang, Z.; et al. Precursor apportionment of atmospheric oxygenated organic molecules using
615 a machine learning method. *Environmental Science: Atmospheres* **2023**, *3* (1), 230-237. DOI:
616 10.1039/d2ea00128d.
617 (37) Stark, H.; Yatavelli, R. L. N.; Thompson, S. L.; Kang, H.; Krechmer, J. E.; Kimmel, J. R.;
618 Palm, B. B.; Hu, W.; Hayes, P. L.; Day, D. A.; et al. Impact of thermal decomposition on
619 thermal desorption instruments: Advantage of thermogram analysis for quantifying volatility
620 distributions of organic species. *Environ Sci Technol* **2017**, *51* (15), 8491-8500. DOI:
621 10.1021/acs.est.7b00160.
622 (38) Zhang, X.; Ye, C.; Kim, J.; Lee, H.; Park, J.; Jung, Y.; Hong, H.; Fu, W.; Li, X.; Chen, Y.;
623 et al. Tropospheric NO2 Column over Tibet Plateau According to Geostationary Environment
624 Monitoring Spectrometer: Spatial, Seasonal, and Diurnal Variations. *Remote Sensing* **2025**, *17*
625 (10). DOI: 10.3390/rs17101690.
626 (39) Liu, Z.; Guo, F.; Zhang, Y.; Wu, Z.; Lu, X.; Deng, J.; Chen, K.; Wang, Q.; He, M. Impact
627 of Lightning-Induced Nitrogen Oxides Over and Around the Tibetan Plateau on the Tibetan
628 Plateau Ozone Valley. *Journal of Geophysical Research: Atmospheres* **2024**, *129* (1). DOI:
629 10.1029/2023jd039575.
630 (40) Guo, Y.; Gong, D.; Wang, H.; Li, Q.; Wu, G.; Wang, Y.; Cai, H.; Yuan, B.; Wang, B.; Liu,
631 S. C. Sources of elevated organic acids in the mountainous background atmosphere of

southern China. *Science of The Total Environment* **2024**, *914*. DOI: 10.1016/j.scitotenv.2023.169673.

(41) Donahue, N. M.; Kroll, J. H.; Pandis, S. N.; Robinson, A. L. A two-dimensional volatility basis set - Part 2: Diagnostics of organic-aerosol evolution. *Atmospheric Chemistry and Physics* **2012**, *12* (2), 615-634. DOI: 10.5194/acp-12-615-2012.

(42) Mehra, A.; Canagaratna, M.; Bannan, T. J.; Worrall, S. D.; Bacak, A.; Priestley, M.; Liu, D.; Zhao, J.; Xu, W.; Sun, Y.; et al. Using highly time-resolved online mass spectrometry to examine biogenic and anthropogenic contributions to organic aerosol in Beijing. *Faraday Discuss* **2021**, *226*, 382-408. DOI: 10.1039/d0fd00080a.

(43) Liang, L. L.; Engling, G.; Liu, C.; Xu, W. Y.; Liu, X. Y.; Cheng, Y.; Du, Z. Y.; Zhang, G.; Sun, J. Y.; Zhang, X. Y. Measurement report: Chemical characteristics of PM2.5 during typical biomass burning season at an agricultural site of the North China Plain. *Atmospheric Chemistry and Physics* **2021**, *21* (4), 3181-3192. DOI: 10.5194/acp-21-3181-2021.

(44) Xu, B.; Tang, J.; Tang, T.; Zhao, S.; Zhong, G.; Zhu, S.; Li, J.; Zhang, G. Fates of secondary organic aerosols in the atmosphere identified from compound-specific dual-carbon isotope analysis of oxalic acid. *Atmospheric Chemistry and Physics* **2023**, *23* (2), 1565-1578. DOI: 10.5194/acp-23-1565-2023.

(45) Khan, M. A. H.; Schlich, B.-L.; Jenkin, M. E.; Shallcross, B. M. A.; Moseley, K.; Walker, C.; Morris, W. C.; Derwent, R. G.; Percival, C. J.; Shallcross, D. E. A Two-Decade Anthropogenic and Biogenic Isoprene Emissions Study in a London Urban Background and a London Urban Traffic Site. *Atmosphere* **2018**, *9* (10). DOI: 10.3390/atmos9100387.

(46) Fang, H.; Wu, T.; Ma, S.; Miao, Y.; Wang, X. Biogenic emission as a potential source of atmospheric aromatic hydrocarbons: Insights from a cyanobacterial bloom-occurring eutrophic lake. *J Environ Sci (China)* **2025**, *151*, 497-504. DOI: 10.1016/j.jes.2024.04.011.

(47) Xu, J. Z.; Zhang, Q.; Wang, Z. B.; Yu, G. M.; Ge, X. L.; Qin, X. Chemical composition and size distribution of summertime PM_{2.5} at a high altitude remote location in the northeast of the Qinghai–Xizang (Tibet) Plateau: insights into aerosol sources and processing in free troposphere. *Atmospheric Chemistry and Physics* **2015**, *15* (9), 5069-5081. DOI: 10.5194/acp-15-5069-2015.

(48) Li, D.; Wang, D.; Caudillo, L.; Scholz, W.; Wang, M.; Tomaz, S.; Marie, G.; Surdu, M.; Eccli, E.; Gong, X.; et al. Ammonium CI-Orbitrap: a tool for characterizing the reactivity of oxygenated organic molecules. *Atmospheric Measurement Techniques* **2024**, *17* (17), 5413-5428. DOI: 10.5194/amt-17-5413-2024.

(49) Isaacman-VanWertz, G.; Massoli, P.; O'Brien, R.; Lim, C.; Franklin, J. P.; Moss, J. A.; Hunter, J. F.; Nowak, J. B.; Canagaratna, M. R.; Misztal, P. K.; et al. Chemical evolution of atmospheric organic carbon over multiple generations of oxidation. *Nature Chemistry* **2018**, *10* (4), 462-468. DOI: 10.1038/s41557-018-0002-2.

(50) Tao, J.; Zhang, Z.; Zhang, L.; Wu, Y.; Ren, Y.; Li, J.; Huang, J.; Wang, G.; Shen, Z.; Zhang, R.; Wang, B. Characterization and sources of water-soluble organic species in PM2.5 in a remote mountain environment in Southeastern China. *Atmospheric Environment* **2023**, *313*. DOI: 10.1016/j.atmosenv.2023.120057.

(51) Mukherjee, S.; Pandithurai, G.; Waghmare, V.; Mahajan, A. S.; Tinel, L.; Aslam, M. Y.; Meena, G. S.; Patil, S.; Buchunde, P.; Kumar, A. Seasonal variability of volatile organic compounds (VOCs) at a high-altitude station in the Western Ghats, India: Influence of biogenic, anthropogenic emissions and long-range transport. *Atmospheric Environment* **2024**, *331*. DOI: 10.1016/j.atmosenv.2024.120598.

(52) Ou-Yang, C.-F.; Chen, Y.-J.; Hsieh, H.-C.; Lee, C.-T.; Chi, K.-H.; Lin, N.-H.; Chang, C.-C.; Wang, J.-L. Identification of organic constituents on atmospheric particulate matter in the East Asian background air of free troposphere by GC×GC-TOFMS. *Chemosphere* **2024**, *364*. DOI: 10.1016/j.chemosphere.2024.143095.

(53) Zhang, Y.; Xu, W.; Zhou, W.; Li, Y.; Zhang, Z.; Du, A.; Qiao, H.; Kuang, Y.; Liu, L.; Zhang, Z.; et al. Characterization of organic vapors by a Vocus proton-transfer-reaction mass spectrometry at a mountain site in southeastern China. *Science of The Total Environment* **2024**, *919*. DOI: 10.1016/j.scitotenv.2024.170633.

(54) Lopez-Hilfiker, F. D.; Iyer, S.; Mohr, C.; Lee, B. H.; D'Ambro, E. L.; Kurtén, T.; Thornton, J. A. Constraining the sensitivity of iodide adduct chemical ionization mass spectrometry to multifunctional organic molecules using the collision limit and thermodynamic stability of iodide ion adducts. *Atmospheric Measurement Techniques* **2016**, *9*

690 (4), 1505-1512. DOI: 10.5194/amt-9-1505-2016.
691 (55) Xu, W.; Bian, Y.; Lin, W.; Zhang, Y.; Wang, Y.; Ma, Z.; Zhang, X.; Zhang, G.; Ye, C.; Xu,
692 X. O3 and PAN in southern Tibetan Plateau determined by distinct physical and chemical
693 processes. *Atmospheric Chemistry and Physics* **2023**, *23* (13), 7635-7652. DOI:
694 10.5194/acp-23-7635-2023.
695 (56) Ye, C. X.; Guo, S. Z.; Lin, W. L.; Tian, F. J.; Wang, J. S.; Zhang, C.; Chi, S. Z.; Chen, Y.;
696 Zhang, Y. J.; Zeng, L. M.; et al. Measurement report: Source apportionment and
697 environmental impacts of volatile organic compounds (VOCs) in Lhasa, a highland city in
698 China. *Atmospheric Chemistry and Physics* **2023**, *23* (18), 10383-10397. DOI:
699 10.5194/acp-23-10383-2023.
700 (57) You, Q. L.; Min, J. Z.; Kang, S. C. Rapid warming in the Tibetan Plateau from
701 observations and CMIP5 models in recent decades. *Int J Climatol* **2016**, *36* (6), 2660-2670.
702 DOI: 10.1002/joc.4520.
703 (58) Ji, Z. M.; Kang, S. C.; Cong, Z. Y.; Zhang, Q. G.; Yao, T. D. Simulation of carbonaceous
704 aerosols over the Third Pole and adjacent regions: distribution, transportation, deposition, and
705 climatic effects. *Clim Dynam* **2015**, *45* (9-10), 2831-2846. DOI: 10.1007/s00382-015-2509-1.
706 (59) Nakayama, T.; Matsumi, Y.; Sato, K.; Imamura, T.; Yamazaki, A.; Uchiyama, A.
707 Laboratory studies on optical properties of secondary organic aerosols generated during the
708 photooxidation of toluene and the ozonolysis of α-pinene. *J Geophys Res-Atmos* **2010**, *115*.
709 DOI: Artn D2420410.1029/2010jd014387.
710 (60) Mehra, A.; Wang, Y.; Krechmer, J. E.; Lambe, A.; Majluf, F.; Morris, M. A.; Priestley, M.;
711 Bannan, T. J.; Bryant, D. J.; Pereira, K. L.; et al. Evaluation of the chemical composition of
712 gas- and particle-phase products of aromatic oxidation. *Atmospheric Chemistry and Physics*
713 **2020**, *20* (16), 9783-9803. DOI: 10.5194/acp-20-9783-2020.
714

715

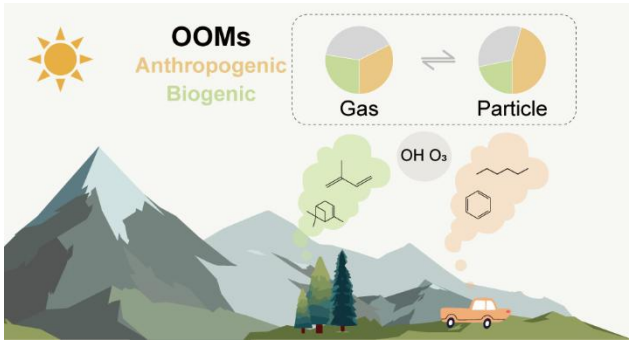

716 **For Table of Contents Only**